Desalination and Water Treatment
www.deswater.com

doi: 10.5004/dwt.2023.29472

291 (2023) 108–116
April

Removal of Mn^{II} and Fe^{III} from groundwater using durian rind-derived biochar

Supamas Danwittayakul[a,*], Woranon Thijina[b]

[a]*National Metal and Materials Technology Center (MTEC), National Science and Technology Development Agency (NSTDA), 111 Thailand Science Park, Thailand Science Park, Klong1, Klong Luang, Pathumthani 12120, Thailand, Tel.: +6625646500 Ext. 4261, email: supamasd@mtec.or.th*
[b]*Interdisciplinary Graduate Program in Advanced and Sustainable Environmental Engineering, Kasetsart University, Bangkok 10900, Thailand, Tel.: +8107041317623; email: woranon.t@ku.th*

Received 11 November 2022; Accepted 14 March 2023

ABSTRACT

In this study, durian rind-derived (DR) biochar was used for Mn^{II} and Fe^{III} removal from aqueous solution. The removal test was conducted on a batch scale with known concentrations of Mn^{II} and Fe^{III} solutions (5–50 mg/L) at pH 2, 4, 7 and 9. The results showed that the precipitation mechanism dominated at basic pH values while adsorption was the main mechanism under acidic conditions. Langmuir and Freundlich adsorption isotherms were used in this study to identify the adsorption behavior. The maximum adsorption capacities of Mn^{II} and Fe^{III} by the biochar were 24.16 and 16.92 mg/g, respectively. The maximum adsorption ability of Mn^{II} onto the biochar was higher than that of Fe^{III}, which was attributed to the ionic radius and electronegativity of metal ions. Two groundwater samples representing Mn^{II}-rich (named HL with 11 mg/L Mn) and Fe^{III}-rich (named RT with 37 mg/L Fe) samples collected from locations close to gold mines were used for the removal tests. Almost 100% of both metals were removed, even under acidic conditions (pH 4). Due to its high efficiency and low cost, DR biochar shows great promise as an attractive adsorbent for metal-ions removal.

Keywords: Groundwater; Adsorption; Precipitation; Durian rind-derived biochar; Gold mine

1. Introduction

Gold mining activities are a known cause of environmental pollution. Gold mine processes have a high potential to generate large amounts of heavy metal ion contaminants in tailing wastewater that create health risks to living things [1]. Typical tailing wastewater contains Mn^{II}, Fe^{III}, Cr^{III}, Ni^{II}, Pb^{II} and Cu^{II}. It is known that these ions have adverse effects on humans. The extent of groundwater contamination in the area has demonstrated that most of the groundwater in gold mining areas is unsuitable for consumption. Thus, the water must be treated prior to utilization [2].

There are several low-cost water treatment technologies generally employed to reduce such contaminants. For instance, ion-exchange, oxidation, filtration, precipitation and adsorption processes have been utilized to remove heavy metal ions [3]. Among the techniques, adsorption is common, inexpensive, easy to operate and widely used. Biochar has been attractive due to its availability and efficiency in heavy metal removal. The utilization of biomass waste such as wheat husk, cotton husk, rice husk, and sawdust to produce biochar offers an advantage because it turns waste into a valuable product [4,5]. Several research studies have focused on the adsorption of metal ions from contaminated water on biochar. Tyagi [6] investigated the adsorption of multiple metal ions using *Vetiveria zizanioides*-derived biochar in a fixed bed column at pH 2–6. They reported maximum adsorption capacities of 139, 130, and 123 mg/g for Pb^{II}, Cu^{II}, and Ni^{II}, respectively. Wang et al. [7] used cotton straw-derived biochar for the adsorption of Pb^{II} from water and found that the maximum Pb^{II} adsorption capacity was 124.7 mg/g at pH 5.5. Vaghetti et al. [8] used nutshell

* Corresponding author.

1944-3994/1944-3986 © 2023 Desalination Publications. All rights reserved.

biosorbent to remove Mn^{II}, Cu^{II} and Pb^{II} from aqueous solutions and found that the maximum adsorption capacities of the sorbent were 97.8, 85.79 and 196.01 mg/g for Mn^{II}, Cu^{II} and Pb^{II}, respectively. Tannic acid-modified activated carbon was used to remove Mn^{II}, Fe^{III}, Cu^{II}, Cd^{II}, and Zn^{II} with adsorption capacities of 1.13, 1.77, 2.23, 1.51 and 1.23 mg/g, respectively [9]. Most of the studies on metal-ion removal have reported on adsorption mechanisms. However, information on the precipitation process, which always takes place simultaneously with adsorption, especially under basic conditions, is still lacking.

Durian is called the king of fruits and is mostly cultivated in Thailand, Indonesia, Malaysia, Cambodia, and Vietnam. Durian has a distinctive strong odor and thorn-covered rind. The covered rind of durians cannot be eaten and becomes biowaste. Thailand is the largest durian producer, producing approximately 600–1,500 kilotons/y, and its rinds become a large amount of waste that needs to be sustainably managed. There are many ways to utilize the durian rind, such as conversion to biofuel, fertilizer, and biochar [10].

Here, we focused on the removal of Mn^{II} and Fe^{III} ions from aqueous systems using durian rind-derived (DR) biochar. The removals of a single system of Mn^{II} and Fe^{III} at pH 2, 4, 7 and 9 by the biochar were investigated. The precipitation mechanism at those pH values was considered as well as the adsorption process. Langmuir and Freundlich adsorption isotherms were used to study the adsorption behavior. Two groundwater samples collected from sources near gold mines in Thailand were tested to investigate the adsorption performance of the DR biochar. One sample was Mn^{II} rich, and the other was Fe^{III} rich.

2. Experimental set-up

2.1. Materials and chemicals

The DR biochar was prepared by a vertical tubular furnace under a N_2 atmosphere. Durian rinds were dehumidified and pyrolyzed in a furnace with a 200 mL/min N_2 (99.99%) flow rate at approximately 600°C for 1 h. The 200 g of as-received biochar was ground, sieved through a 750 mm mesh, soaked in 0.1 M HNO_3 and washed with deionized water several times followed by drying at 110°C. Mn^{II} and Fe^{III} standard solutions were analytical grade and supplied by Perkin Elmer. High purity water (18.2 MOhm) was used throughout this work. Groundwater was collected from 2 locations close to the Phu Tap Fa (latitude and longitude: 17.3522363 and 101.6574528) and Chatree (latitude and longitude: 16.262174 and 100.6534) gold mines in northeastern and northern Thailand, respectively. Among those samples, 2 samples were selected for use in this study due to their high Mn and Fe contents, labeled HL and RT, respectively. The samples were stored at 4°C before use. 1 L of each water sample was stabilized by adding 5 mL of 65 wt.% nitric acid for elemental analysis by inductively coupled plasma-optical emission spectroscopy (ICP-OES, Horiba, Activa).

2.2. Characterization of biochar

The specific surface area and average pore size of the DR biochar were investigated using N_2 adsorption–desorption isotherm analysis (Quantachrome, Autosorb-1C). The morphology of the DR biochar was characterized using field emission scanning electron microscopy (FE-SEM; Hitachi, SU-8030) operating at 5 kV. The contents of carbon, hydrogen, nitrogen, and sulfur in biochar were examined by a CHNS analyzer (Leco, TruSpec Micro). The pH values of the samples were determined by the inhouse method of the Pacific Northwest National Lab by mixing 1 part biochar to 20 parts water, stirring the mixture for 3 h, and determining the pH of the sample solution [11]. The water contact angle (WCA) of the biochar was determined using a water contact angle instrument, DataPhysics Instrument, 0CA40. Surface functional group analysis of the biochar was performed using a Fourier-transform infrared (FTIR) spectroscope (Shimadzu, IR Prestige-21 with ATR mode) as well as Boehm titration [12]. Its point of zero charge was measured by using a zeta potential analyzer (Malvern, Zetasizer Nano ZSP).

2.3. Metal ion removal

A batch test was carried out to determine the performance of the DR biochar in the removal of Mn^{II} and Fe^{III} from water. A series of Mn^{II} and Fe^{III} aqueous solutions at concentrations of 0, 5, 15, 25, 35 and 50 mg/L in deionized water were prepared at pH 2, 4, 7 and 9. The pH values of the solution were adjusted by 0.1 M of HNO_3 or NaOH. Each experiment was conducted at room temperature (25°C) in a 100 mL beaker. 50 mL of each metal ion solution (at a tested concentration and pH) was added, followed by the addition of 50 mg of DR biochar in a constant stirring system. After 24 h, the mixture was filtered using Whatman filter paper (grade 3) to collect the filtrate. Metal ions remaining in the solution were determined by ICP-OES. The total removal percentage (R) was calculated using Eq. (1):

$$R = \frac{C_i - C_f}{C_i} \times 100 \tag{1}$$

where C_i and C_f are the initial and equilibrium concentrations of metal ions, respectively (mg/L).

Mn^{II} and Fe^{III} are easily oxidized especially under basic conditions, forming solid particles [13]. The precipitation of the products needs to be considered in the removal process. Separate precipitation experiments of each metal ion were carried out by stirring 50 mL of metal ion solution at each concentration and pH for 24 h without biochar. The rest of the protocol was followed as mentioned above. The percentage of precipitation removal (P) was calculated using Eq. (2):

$$P = \frac{C_i - C_p}{C_i} \times 100 \tag{2}$$

where C_i is the initial concentration of metal ions and C_p is the metal ion concentration after the precipitation test.

Metal ion adsorption (A) was calculated from the subtraction of the total removal with the precipitation removal using Eq. (3), and the quantity of metal ions adsorbed onto the biochar can be calculated as Eq. (4).

$$A = T - P = \frac{\left(C_i - C_f - C_p\right)}{C_i} \times 100 \quad (3)$$

$$q_e = \frac{V\left(C_i - C_f - C_p\right)}{m} \quad (4)$$

where q_e (mg/g) is the experimental adsorption capacity of metal ions, V (L) is the volume of the tested solution and m (g) is the mass of the adsorbent.

2.4. Groundwater from the gold mine

Metal ion removal (Mn^{II} and Fe^{III}) from the groundwater samples, HL and RT, using the DR biochar was also investigated at pH 4, pH 7 and pH 9. The HL sample represented Mn^{II}-rich water, and the RT sample represented Fe^{III}-rich water. %Total removal, precipitation removal and adsorption removal were calculated as mentioned above. Each condition was repeated for 4 replicates.

3. Results and discussion

3.1. Characterization of the DR biochar

The physico-chemical properties of the DR biochar are summarized in Table 1. The average pore size of the DR biochar was 2.6 nm with a specific surface area of 170 m^2/g and pore volume of 0.11 cm^3/g. The N_2 adsorption–desorption isotherm of the DR biochar was classified as Type II of the IUPAC classification indicating that multilayer adsorption dominated (Supplementary Information) [14]. The H/C atomic ratio was used as an index for reflecting the aromaticity of biochar and for predicting the sorption properties of biochar. The H/C of the DR biochar was 0.215, showing that it had a sufficient amount of fused aromatic hydrocarbon as the main characteristic of biochar [15] and was in the range of high adsorption capacity [16].

The FTIR spectrum corresponded to the Boehm results that there was a C=O peak at 1,629 cm^{-1} of the carboxylic group, a 1,398 cm^{-1} peak of phenolic O–H bending, and a C–H stretching vibration of aliphatic compounds (Supporting information) [17]. Surface functionality by the Boehm method showed the existence of phenolic, lactonic and carboxylic functional groups of 91, 33 and 21 mmol/g, respectively. This confirmed that the biochar was suitable for sorption applications.

The water contact angle (WCA) of the DR biochar was 59, which was less than 90°, indicating that the biochar had hydrophilic behavior. The pH of the DR biochar was 10.25 with a zetapotential of –37.8 mV. The plot of the zetapotential against pH was in the negative range (Supporting information). This indicated that the electrostatic force between the negative charge on the biochar surface and metal cations followed the adsorption mechanism. The point of zero charge of the biochar was in the acidic range below pH 2.

3.2. Elemental contents of the groundwater samples

The groundwater samples, HL and RT, were elemental analyzed by ICP-OES, and the results are summarized in Table 2. The HL sample was a representative Mn-rich (11.1 mg/L) sample accompanied by high salt contents (20 mg/L Mg, 80 mg/L Ca and 318 mg/L Na), while RT was the Fe-rich (37.4 mg/L) sample. The pH of HL was 7.0, and that of RT was 7.4, and the total organic carbon (TOC) contents of HL and RT were 13.7 and 10.4, respectively.

3.3. Metal ion removal

The results of the removal efficiencies of Mn^{II} and Fe^{III} by the DR biochar with varying initial metal concentrations

Table 1
Physico-chemical properties of the durian rind biochar

Characteristics of the durian rind biochar	Value
Brunauer–Emmett–Teller specific surface area (m^2/g)	169.84
Pore volume (cm^3/g)	0.111
Average pore diameter (nm)	2.62
H/C_{org} (molar ratio)	0.215
C (wt.%)	91.66
N (wt.%)	0.37
S (wt.%)	0.48
pH	10.25
Zeta potential (mV)	–37.8
Carbon surface functionality (n_{CSF} (umol/g))	
- Phenolic	91.1
- Lactonic	33.4
- Carboxylic	21.0
Water contact angle	59

$N = 4$

Table 2
Elemental analysis of the groundwater samples by inductively coupled plasma-optical emission spectroscopy

Water sample	pH	TOC (mg/L)	Elemental concentrations									
			mg/L							μg/L		
			Mn	Fe	Mg	Ca	Na	K	S	Zn	Cu	As, Cr, Pb, Cd
HL	7.03	13.7	11.1	0.8	20.3	79.5	318.1	62.8	112.4	21	53	<5 μg/L
RT	7.41	10.4	1.5	37.4	3.8	7.6	4.1	3.2	2.9	37	55	<5 μg/L

The detection limits of inductively coupled plasma-optical emission spectroscopy for As, Cr, Pb and Cd were 5 μg/L.

ranging from 5–50 mg/L are shown in Figs. 1 and 2, respectively. In this study, we determined the total metal-ion removal amount from both the precipitation of metal ions and the adsorption process. Fig. 1a illustrates the total removal of Mn^{II} (gray), Mn^{II} removed by precipitation (blue) and Mn^{II} removed by adsorption (yellow) at pH 2. At a low initial Mn^{II} concentration (5 mg/L), 48% Mn^{II} total removal was obtained while at a high Mn^{II} concentration (50 mg/L), only 17% Mn^{II} removal was achieved. Under highly acidic conditions, Mn^{II} prefers to be a free ion rather than forming particles or being adsorbed on the sorbent surface [13,18], resulting in low removal efficiencies. Fig. 1b shows that at pH 4 and an initial concentration of 5 mg/L Mn^{II} solution, 98% of Mn^{II} ions were removed. A total of 66% of 98% was from adsorption, and the remaining 32% was from particle precipitation. The percentage of Mn removal decreased with

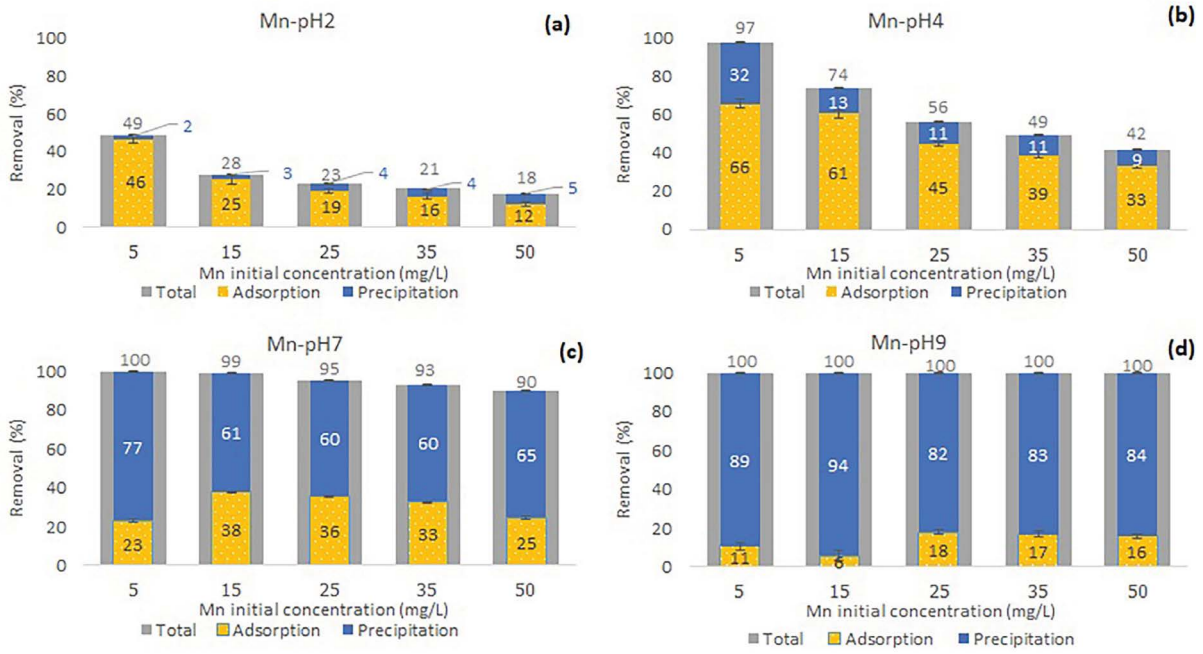

Fig. 1. Bar plots of Mn^{II} removal performance using the durian rind biochar in Mn^{II} solution; (a) pH 2, (b) pH 4, (c) pH 7 and (d) pH 9.

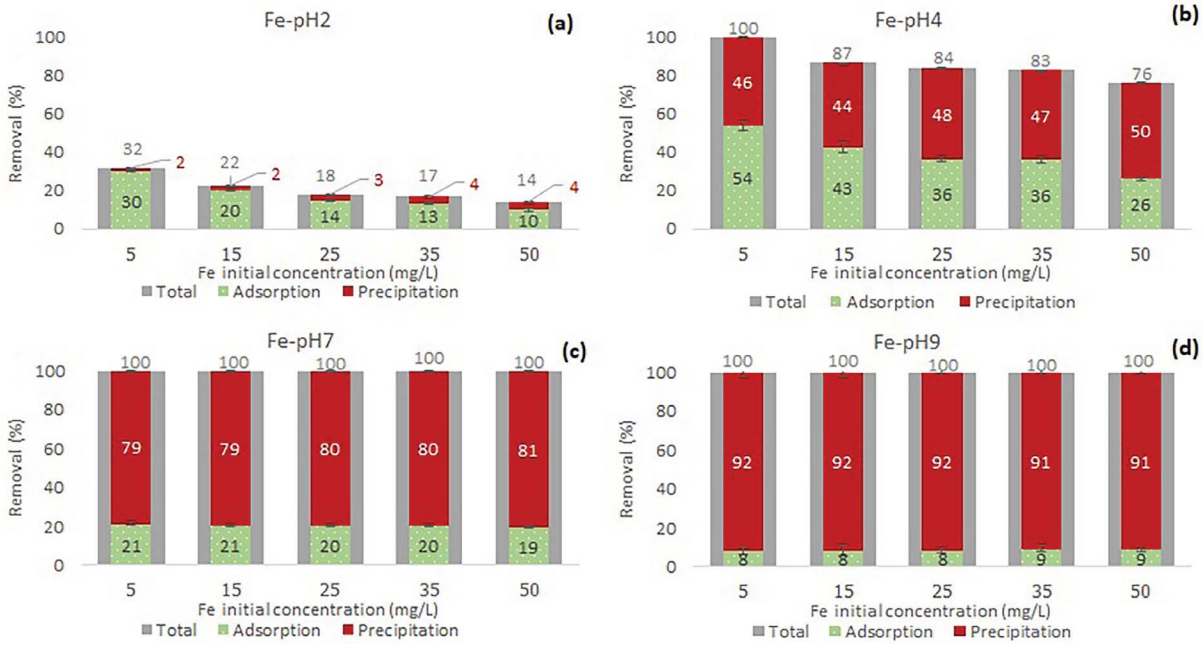

Fig. 2. Bar plots of Fe^{III} removal performance using durian rind biochar in Fe^{III} solution; (a) pH 2, (b) pH 4, (c) pH 7 and (d) pH 9.

increasing Mn concentration due to an insufficient number of adsorption sites compared to the amount of Mn^{II} ions in the solution. In addition, Mn^{II} ions at pH 4 tend to start forming oxide or hydroxide particles more than those at pH 2, resulting in a higher precipitation percentage. At pH 7 (Fig. 1c), the Mn^{II} removals were above 90% at all studied concentrations with a relatively high precipitation percentage (≤60%), while approximately 23–39% of Mn^{II} ions were removed by adsorption. At pH 9, the total Mn removal was higher than 99% of all Mn^{II} at initial concentrations (5–50 ppm). More than 82% of 99% Mn^{II} removal was due to the precipitation process, and only 6%–18% was from adsorption removal. Here, we summarize that under acidic conditions (pH 2–4), adsorption removal dominated, while at pH ≥ 7, the main mechanism became precipitation.

Similar results were found with the removal test of Fe^{III} ions using DR biochar (Fig. 2). At pH 2 (Fig. 2a), the highest Fe^{III} removal was found at 5 mg/L Fe^{II} solution, with 32% total Fe^{III} removal (gray), 30% from adsorption (green) and less than 2% from precipitation (red). At pH 4, approximately 45%–50% of Fe^{III} ions were removed by the precipitation process, while the remaining Fe^{III} ions were adsorbed by the DR biochar depending on the number of adsorption sites and the number of free metal ions. The highest adsorption efficiency was 54% when the initial Fe^{III} concentration was 5 mg/L. At pH 7, a total Fe^{III} removal of nearly one hundred percent was achieved from 80% precipitation of Fe^{III} compounds and approximately 20% from adsorption. At pH 9, the total Fe^{III} removal also achieved 100% with >90% precipitation, and the rest of the ions were removed by adsorption. Comparing the removal of Mn^{II} and Fe^{III} from aqueous solution, it could be observed that Fe^{III} formed solid particles easier than Mn^{II} at the same pH, which was in agreement with their chemical potential [18–20].

The experimental results supported the characteristics of the DR biochar that it has high adsorption ability. The isoelectric point of the DR biochar was below pH 2, and the zeta potentials were all negative, indicating that there was a high electrostatic interaction between the negative charge of the biochar surface and metal cations over a wide pH range. In addition, the surface functional groups of the biochar including lactonic, carboxylic and phenolic groups, also promoted the adsorption of metal ions on the biochar surfaces by their dangling bonds. Moreover, the hydrophilic surface (low contact angle) of the biochar enhanced the accessibility of the metal ions to the adsorption sites. The surface treatment of the biochar by nitric acid was a key to unveiling the surface for aqueous applications.

3.4. Adsorption isotherms of Mn^{II} and Fe^{III}

To evaluate the adsorption potential of Mn^{II} and Fe^{III} by the DR biochar, the adsorption capacity (q_e) of each metal ion at pH 4 was plotted against their initial concentration after the subtraction of precipitation results as shown in Fig. 3. It was observed that the adsorption capacity increased with increasing initial ion concentration. At low concentrations, there were plenty of adsorption sites on the outer surface of biochar, and metal ions could freely occupy such free adsorption sites by electrostatic attraction. At higher initial concentrations, the rest of the metal ions moved randomly to find unoccupied sites in the inner surface of the biochar, or they possibly adsorbed on top of the occupied sites forming multilayer adsorption, resulting in an increase in adsorption capacity.

Langmuir and Freundlich adsorption isotherms were applied to estimate the maximum adsorption capacities and used to describe the adsorption behavior of Mn^{II} and Fe^{III} on the DR biochar. By fitting the experimental data, the linear plots for Mn^{II} and Fe^{III} are shown in Figs. 4 and 5, and the main adsorption parameters are given in Table 3. The relative R^2 of more than 0.95 suggested that both the Langmuir and Freundlich isotherms were fitted well with the experimental data of Mn^{II} with R^2 values of 0.987 and 0.976, respectively, while only the Langmuir model was fitted with Fe^{III} experimental results of 0.977 R^2. The Langmuir fitting model revealed that the maximum adsorption capacity of the DR biochar for Mn^{II} was 24.16 mg/g, while that of Fe^{III} was 16.92 mg/g. The K constant of Fe^{III} was 0.326 and 0.046 for Mn^{II}, indicating that the interaction of Fe^{III} onto the DR biochar was much stronger than that of Mn^{II}. The DR biochar had a higher adsorption capacity for Fe^{III} than for Mn^{II}. This might be related to the electronegativity of adsorbates. The electronegativity of Fe (1.8) is higher than that of Mn (1.5). In fact, electronegativity is measured from the strength of the element to attract electrons. However, it could be used to show the tendency of the strength of Fe^{III} and Mn^{II} interacting with negative charges on the biochar surface. An

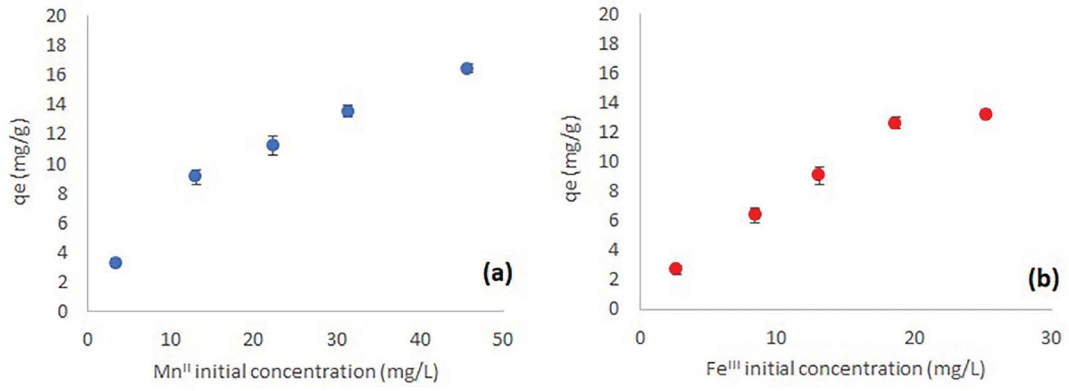

Fig. 3. Adsorption capacity of metal ions: (a) Mn^{II} and (b) Fe^{III} at pH 4 in a single metal system by the durian rind biochar.

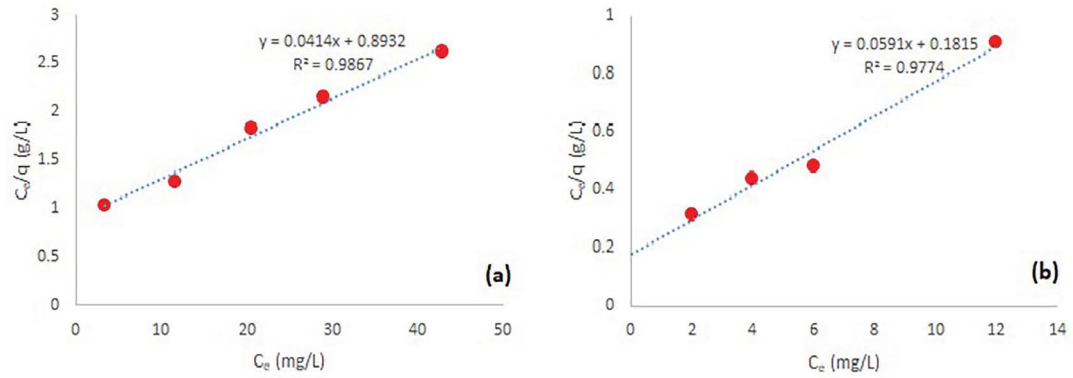

Fig. 4. Langmuir isotherm plots for (a) Mn^{II} and (b) Fe^{III}.

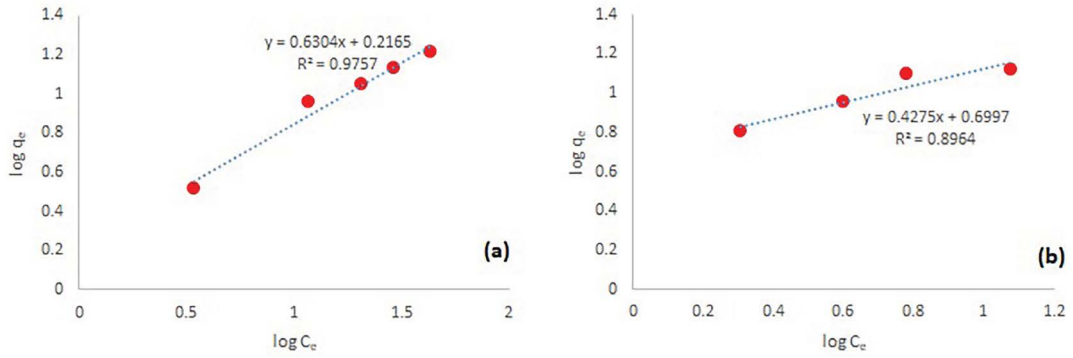

Fig. 5. Freundlich isotherm plots for (a) Mn^{II} and (b) Fe^{III}.

Table 3
Mn^{II} and Fe^{III} adsorption capacity of the durian rind biochar

Heavy metal	Langmuir isotherm			Freundlich isotherm		
	K_L	q_m (mg/g)	R^2	K_f	n	R^2
Mn	0.046	24.16	0.9867	1.646	1.586	0.9757
Fe	0.326	16.92	0.9774	5.008	2.339	0.8964

additional factor that could contribute to different K_L and K_f results on metal ions is the ionic radius. Fe^{III} has a smaller ionic radius than Mn^{II} therefore, Fe^{III} has a higher attractive force than Mn^{II} [21]. Such a small ionic radius of Fe^{III} creates a higher potential to penetrate the micropores of the biochar. All of these reasons supported that Fe^{III} ions could balance the negative electrostatic attraction on the biochar surfaces faster than Mn^{II} ions, leading to Mn^{II} having a higher maximum adsorption capacity.

The Freundlich constants K_f and n were found to be 1.646 mg/g and 1.586 for Mn and 5.008 mg/g and 2.339, respectively, for Fe. The K_f of Fe^{III} was much higher than that of Mn^{II}. This was in agreement with the results obtained by the Langmiur plot, confirming the higher interaction between the heterogeneous surface of DR biochar and Fe^{III} than that of Mn^{II}. In this study, n values were greater than one ($n > 1$) reflecting a high affinity between the adsorbent and adsorbate [22]. The conformity of the adsorption data to the Freundlich isotherm (correlation coefficient, $R^2 > 0.9$) exhibited a complex multilayer adsorption process or multiple site type of binding [23].

Table 4
Previously reported adsorption capacities for various adsorbents for metal ion adsorption

Adsorbent	Adsorption capacity (mg/g)		References
	Mn^{II}	Fe^{III}	
Silica gel modified with salicylaldoxime	–	2.8	[26]
Tannic acid immobilized activated carbon	1.13	1.77	[9]
Acrylonitrile grafted banana peel	5.73	–	[24]
	2.55	3.60	
Natural zeolitic tuff	10	–	[25]
Durian rind biochar (This work)	24.16	16.92	This work

The highest metal-ion removal percentages of this study are compared with results obtained from other reports in the literature, as shown in Table 4. The results indicated that a 1.13 mg/g Mn^{II} adsorption capacity was achieved

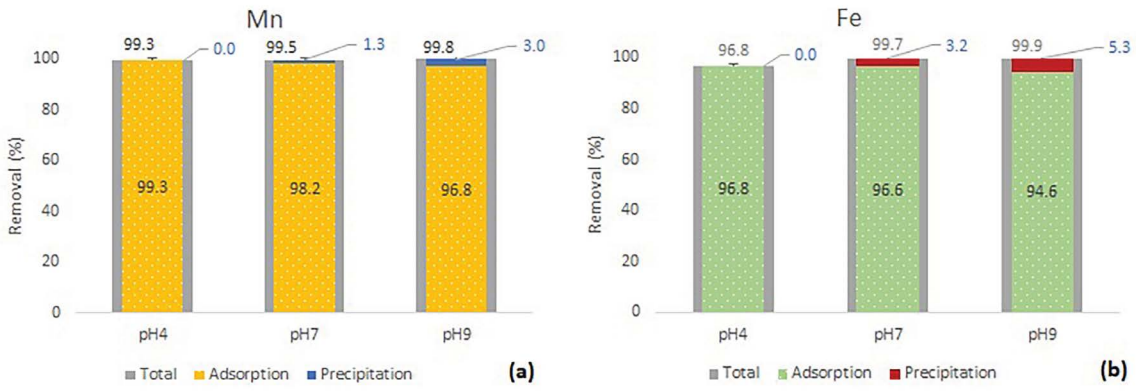

Fig. 6. Removal of metal ion from real groundwater using the durian rind biochar at pH 4, pH 7 and pH 9; (a) Mn from HL and (b) Fe from RT.

using tannic acid-immobilized activated carbon [9], while 5.73 and 10 mg/g Mn^{II} adsorption capacities were achieved using acrylonitrile-grafted banana peel [24] and natural zeolitic tuff [25], respectively. In comparison, our DR biochar showed a maximum adsorption capacity of 24.16 mg/g Mn^{II}. For Fe^{III} adsorption, silica gel modified with salicylaldoxime exhibited a maximum adsorption capacity of approximately 2.8 mg/g [26], while maximum adsorption capacities of 1.77 and 3.60 mg/g Fe^{III} were obtained using tannic acid-immobilized activated carbon and natural zeolitic tuff, respectively. Their results were low compared to our adsorption capacity results of 16.92 upon using the DR biochar. This might be attributed to the high surface functionality, high surface area and high wettability of the DR biochar.

3.5. Application to groundwater

The removal of Mn^{II} and Fe^{III} from real groundwater at pH 4, pH 7 and pH 9 using DR biochar is shown in Fig. 6. Above 99% metal removal was obtained in all experiments. The results showed that at pH 4, the total Mn^{II} and Fe^{III} removals were only due to an adsorption mechanism with only a small percentage from precipitation. This was in strong contrast to the above results obtained from Mn^{II} or Fe^{III} solutions. We found that the adsorption mechanism dominated because the groundwater samples contained high complex ions of salts and TOCs. Foreign ions could inhibit precipitation through the deflocculation process via electrostatic stabilization [27]. In addition, TOCs in the system could enhance adsorption ability by forming metal organic compounds as well [28].

4. Conclusions

The DR biochar contained various functional groups, such as lactonic, carboxylic and phenolic groups, which behaved as active sites for the adsorption of metal ions. The removal efficiencies of Mn^{II} and Fe^{III} by the DR biochar were almost 100% at high pH (pH 9) due to the precipitation mechanism, while at low pH, the adsorption process dominated. The adsorption behavior was well fitted with the Langmuir isotherm, with the maximum adsorption capacities of Mn^{II} and Fe^{III} being 24.16 and 16.92 mg/g, respectively. The Freundlich constants explained the better maximum adsorption capacity of Mn^{II} for the DR biochar than that of Fe^{III} due to the ionic radius and electronegativity. The DR biochar performed approximately 100% metal removal from the complex groundwaters with high heavy metal and salt contents at all studied pH values. High-efficiency and low-cost DR biochar can be an alternative option for commercial adsorbents for the removal of toxic heavy metals from groundwater or wastewater.

Acknowledgements

The authors would like to acknowledge partial financial support from the P1750394 project and National Metal ans Materials Technology Center (MTEC), National Science and Technology Development Agency (NSTDA), Thailand. We are thankful to Prof. Dr. Supapan Seraphin, Professional Authorship Center, NSTDA, for invaluable suggestions on manuscript preparation.

References

[1] H. Ding, L. Tang, Y. Nie, H. Ji, Characteristics and interactions of heavy metals with humic acid in gold mining area soil at a upstream of a metropolitan drinking water source, J. Geochem. Explor., 200 (2019) 266–275.
[2] M.M. Manyuchi, N. Sukdeo, W. Stinner, T.N. Mutusva, Influence of sawdust based biochar on gold tailings wastewater heavy metal contaminants removal, S. Afr. J. Chem. Eng., 37 (2021) 81–91.
[3] L.D. Senanu, G. Kranjac-Berisavljevic, S.J. Cobbina, The use of local materials to remove heavy metals for household-scale drinking water treatment: a review, Environ. Technol. Innovation, 29 (2023) 103005, doi: 10.1016/j.eti.2023.103005.
[4] X. Gu, X. Ma, L. Li, C. Liu, K. Cheng, Z. Li, Pyrolysis of poplar wood sawdust by TG-FTIR and Py-GC/MS, J. Anal. Appl. Pyrolysis, 102 (2013) 16–23.
[5] G. Lin, T. Hu, S. Wang, T. Xie, L. Zhang, S. Cheng, L. Fu, C. Xiong, Selective removal behavior and mechanism of trace Hg(II) using modified corn husk leaves, Chemosphere, 225 (2019) 65–72.
[6] U. Tyagi, Enhanced adsorption of metal ions onto *Vetiveria zizanioides* biochar via batch and fixed bed studies, Bioresour. Technol., 345 (2022) 126475, doi: 10.1016/j.biortech.2021.126475.
[7] Z. Wang, J. Xu, D. Yellezuome, R. Liu, Effects of cotton straw-derived biochar under different pyrolysis conditions on Pb(II)

adsorption properties in aqueous solutions, J. Anal. Appl. Pyrolysis, 157 (2021) 105214, doi: 10.1016/j.jaap.2021.105214.
[8] J.C.P. Vaghetti, E.C. Lima, B. Royer, B.M. da Cunha, N.F. Cardoso, J.L. Brasil, S.L.P. Dias, Pecan nutshell as biosorbent to remove Cu(II), Mn(II) and Pb(II) from aqueous solutions, J. Hazard. Mater., 162 (2009) 270–280.
[9] A. Üçer, A. Uyanik, S.F. Aygün, Adsorption of Cu(II), Cd(II), Zn(II), Mn(II) and Fe(III) ions by tannic acid immobilised activated carbon, Sep. Purif. Technol., 47 (2006) 113–118.
[10] S. Thongkaew, C. Jatuporn, P. Sukprasert, P. Rueangrit, S. Tongchure, Factors affecting the durian production of farmers in the eastern region of Thailand, Int. J. Agric. Ext., 9 (2021) 285–293.
[11] J.E. Amonette, Letter Report for Characterization of Biochar, Pacific Northwest National Lab., Richland, Washington, 2013.
[12] S.L. Goertzen, K.D. Thériault, A.M. Oickle, A.C. Tarasuk, H.A. Andreas, Standardization of the Boehm titration. Part I. CO_2 expulsion and endpoint determination, Carbon, 48 (2010) 1252–1261.
[13] W.G. Whitman, Corrosion of iron, Chem. Rev., 2 (1926) 419–435.
[14] M.D. Donohue, G.L. Aranovich, Classification of Gibbs adsorption isotherms, Adv. Colloid Interface Sci., 76–77 (1998) 137–152.
[15] J.H. Windeatt, A.B. Ross., P.T. Williams, P.M. Forster, M.A. Nahil, S. Singh, Characteristics of biochars from crop residues: potential for carbon sequestration and soil amendment, J. Environ. Manage., 146 (2014) 189–197.
[16] X. Xiao, Z. Chen, B. Chen, H/C atomic ratio as a smart linkage between pyrolytic temperatures, aromatic clusters and sorption properties of biochars derived from diverse precursory materials, Sci. Rep., 4 (2015) 22644, doi: 10.1038/srep22644.
[17] M. Stylianou, A. Christou, P. Dalias, P. Polycarpou, C. Michael, A. Agapiou, P. Papanastasiou, D. Fatta-Kassinos, Physico-chemical and structural characterization of biochar derived from the pyrolysis of biosolids, cattle manure and spent coffee grounds, J. Energy Inst., 93 (2020) 2063–2073.
[18] C.P. Yi, S.R. Majid, The Electrochemical Performance of Deposited Manganese Oxide-Based Film as Electrode Material for Electrochemical Capacitor Application, R. Inguanta, C. Sunseri, Eds., Semiconductors – Growth and Characterization, InTechOpen, 2018, pp. 133–158.
[19] J.E. van Benschoten, W. Lin, W.R. Knocke, Kinetic modeling of manganese(II) oxidation by chlorine dioxide and potassium permanganate, Environ. Sci. Technol., 26 (1992) 1327–1333.
[20] H.-H. Huang, The Eh-pH diagram and its advances, Metals, 6 (2016) 23, doi: 10.3390/met6010023.
[21] A. bin Jusoh, W.H. Cheng, W.M. Low, A. Nora'aini, M.J.M.M. Noor, Study on the removal of iron and manganese in groundwater by granular activated carbon, Desalination, 182 (2005) 347–353.
[22] J.Q. Jiang, C. Cooper, S. Ouki, Comparison of modified montmorillonite adsorbents Part I: preparation, characterization and phenol adsorption, Chemosphere, 47 (2002) 711–716.
[23] R.S. Bai, T.E. Abraham, Studies on chromium(VI) adsorption–desorption using immobilized fungal biomass, Bioresour. Technol., 87 (2003) 17–26.
[24] A. Ali, Removal of Mn(II) from water using chemically modified banana peels as efficient adsorbent, Environ. Nanotechnol. Monit. Manage., 7 (2017) 57–63.
[25] N. Rajic, D. Stojakovic, S. Jevtic, N.Z. Logar, J. Kovac, V. Kaucic, Removal of aqueous manganese using the natural zeolitic tuff from the Vranjska Banja deposit in Serbia, J. Hazard. Mater., 172 (2009) 1450–1457.
[26] A.R. Sarkar, P.K. Datta, M. Sarkar, Sorption recovery of metal ions using silica gel modified with salicylaldoxime, Talanta, 43 (1996) 1857–1862.
[27] A.L. Johnson, F.H. Norton, Fundamental study of clay: II, mechanism of deflocculation in the clay-water system, J. Am. Ceram. Soc., 24 (1941) 189–203.
[28] J. McLean, B. Bledsoe, Behavior of Metals in Soils, U.S. Environmental Protection Agency, Washington, D.C., EPA/540/S-92/018 (NTIS PB93131480), 1992.

Supporting information

S1. Physico-chemical of the durian rind biochar

The average pore size of the durian rind (DR) biochar was 2.6 nm with the specific surface area of 170 m^2/g and pore volume of 0.11 cm^3/g. The N_2 adsorption–desorption isotherm of the DR biochar was classified as Type II of IUPAC classification indicated that the multilayer adsorption was dominated (Fig. 1) [14].

Fourier-transform infrared spectrum corresponded to the Boehm results that there was C=O peak at 1,629 cm^{-1} of carboxylic group, 1,398 cm^{-1} peak of phenolic O–H bending, C–H stretching vibration of aliphatic compounds (Fig. 2) [19].

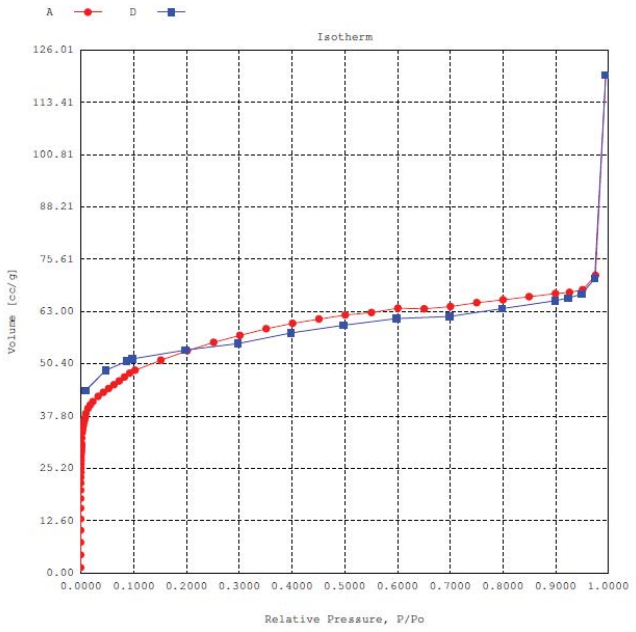

Fig. 1. Adsorption–desorption isotherm of the durian rind biochar.

Plot of zetapotential against pH were in the negative range (Fig. 3). This indicated that electrostatic force between the biochar negatively surface charge and positively charge of metal ion be involved in the adsorption mechanism. The point of zero charge of the biochar was at below pH 2.

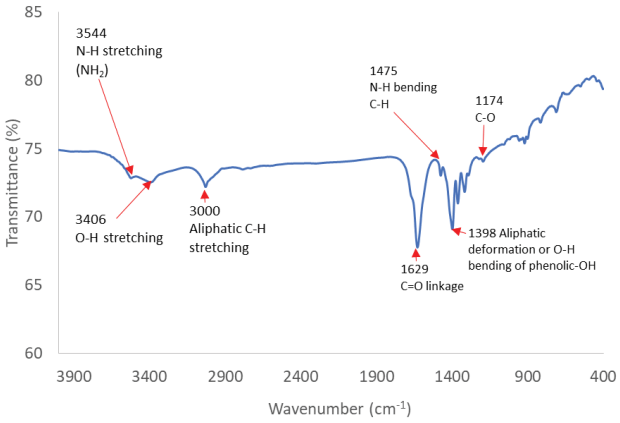

Fig. 2. Fourier-transform infrared spectrum of the durian rind biochar from 400–4,000 cm^{-1}.

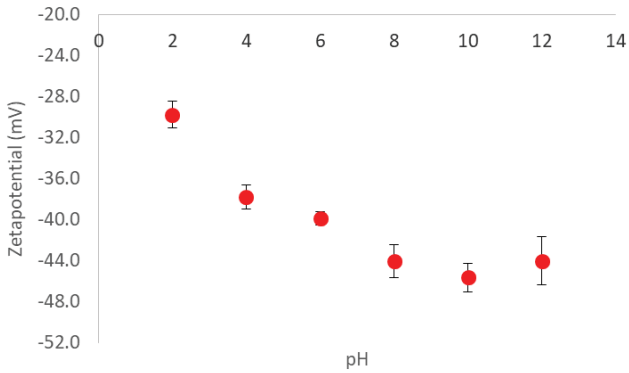

Fig. 3. Plot of zetapotential vs. pH.